Journal of Applied and Natural Science
15(1), 107 - 115 (2023)
ISSN : 0974-9411 (Print), 2231-5209 (Online)
journals.ansfoundation.org

Research Article

Spectral signatures for iron ore deposits in Tirthamalai area, Dharmapuri District, Tamil Nadu, India

Cendrayan Kasilingam*
Department of Geology, Periyar University, Salem (Tamil Nadu), India
Arisiyappan Thirunavukkarasu
Department of Geology, Periyar University, Salem (Tamil Nadu), India
Chandran Ramachandran
Department of Geology, Periyar University, Salem (Tamil Nadu), India

*Corresponding author. Email: kasigeo02@gmail.com

Article Info
https://doi.org/10.31018/jans.v15i1.4160
Received: November 3, 2022
Revised: January 28, 2023
Accepted: February 2, 2023

How to Cite
Kasilingam, C. *et al.* (2023). Spectral signatures for iron ore deposits in Tirthamalai area, Dharmapuri District, Tamil Nadu, India. *Journal of Applied and Natural Science*, 15(1), 107 - 115. https://doi.org/10.31018/jans.v15i1.4160

Abstract
The demand for iron ore has increased recently and employing geochemical and hyperspectral remote sensing techniques for discovering new ore and mineral resources have primarily been concentrated on the economic phases. The present study aimed to characterize the hyperspectral spectral signatures of iron ores of field samples to map the deposits that occurred in the Tirthamalai hill region, which lies in the parts of Harur Taluk, Dharmapuri district of Tamil Nadu state, India The measurement and study of spectral signatures of the different samples of the deposits showed strong spectral absorptions near 500 nm, 900 nm and 2400 nm wavelength regions and were confirmed with the Fourier Transform Infrared (FTIR) spectroscopy method. The spectral absorption characteristics of the samples were evaluated by the study of the physical, optical, and chemical characteristics of the samples. The study of hyperspectral and FTIR spectral signatures with petrographic and major chemical elements revealed the best absorption characteristics of the iron ore deposits of the study region and can be used elsewhere in the world. This report presents preliminary findings on the use of hyperspectral imaging to characterize iron ore. The mineralogical products produced from hyperspectral images may improve in situ grade control on an iron ore mine face. It will be extremely useful for businesses in measuring large numbers of commodities quickly and objectively.

Keywords: FTIR, Geochemistry, Iron Formation, Spectral Signatures, Tirthamalai region

INTRODUCTION

Hyperspectral remote sensing at high spectral and hyperspectral resolution provides detailed physicochemical information about Earth's surface (mineralogy, chemistry, and morphology) (Baissa *et al*., 2011; Raja *et al*., 2010; Khan *et al*., 2018). Such information is valuable for mapping rocks with different mineral compositions, potential hosts of ore mineralization, metasomatic mineral associations, etc. and has become indispensable part of geological research. The near-infrared and mid-infrared (0.3 to 2.5 m) and spectral regions of the electromagnetic spectrum are covered by the hyperspectral sensors and tens to hundreds of small adjacent spectral bands are used to record the electromagnetic energy reflected of the Earth's surface (Ganesh *et al*. 2004).The study of spectral data in the visible and near-infrared (VNIR) spectral ranges is expedient for the fast interpretation of satellite images (Abubakar *et al*. 2019). Because these wavelengths are diagnostic for a wide variety of interactions between electromagnetic energy and the rock material, VNIR is among the most useful wavebands for mapping rock surface mineralogy, which is influenced by significant physical and chemical characteristics. Other essential factors are the rock surface's structure, texture, and modified state (Ortenberg, 2018).

The iron ore deposits of Tamil Nadu, India, are confined to the high-grade mobile belts represented by oxide facies iron formations. The deposits are in the group of Precambrian iron formations occurring as narrow, highly deformed, and metamorphosed belts within the Archaean granulite terrain. The deposits are older than > 3000 Ma (Sylvestre *et al*., 2017). These are banded magnetite quartzite differentiated based on enriched minerals of magnetite (Fe_3O_4) and quartz (SiO_2), having an iron content of 35-40% low-grade iron ores (Jha, 2021). The deposits are amenable to mag-

netite concentration and exploitable while using the cost -effective beneficiation technique (Bodsworth, 2018; Roonwal, 2018). The present study characterized the hyperspectral absorption characteristics of the iron ore samples of the Tirthamalai hill region using the spectroscopy method to understand the absorption characteristics of the iron ores and use the knowledge to map iron ore deposits of the world.

MATERIALS AND METHODS

Study area

The study region in and around Tirthamalai hill (latitudes N 12° 03'and 12° 06' and longitudes E 78° 35' and 78° 38') in Dharmapurai District, Tamil Nadu, India is a part of the Archaean Peninsular complex having intensive high-grade regional metamorphism (Santosh *et al*., 2009; Tsunogae and Santosh, 2010; Santosh, 2015) with folding, faulting and shearing structures. The major rock types in the area include banded magnetite quartzite, charnockite and epidote hornblende gneiss (Fig. 1). There are four significant bands of magnetite quartzite formations which traverse Tirthamalai hill. The iron formations of Tirthamalai hill are dark colored and strongly banded. The banding is due to the silica and silicate, and iron-rich oxide minerals show alternate light and dark-colored layers. The major minerals are magnetite and quartzite of meta-sedimentary origin. The magnetite quartzites have been classified based on grain size as 1. Fine-grained size, 2. Medium-grained size, 3. Coarse-grained size (Rajendran *et al*., 2011; Thirunavukkarasu *et al*., 2015).

In the present study, the spectral absorption characters of banded magnetite iron ores of study region were studied by collection of spectral signatures using portable Ground Truth Hyperspectral Spectroradiometer of Analytical Spectral Devices (ASD, Field Spec 3) working in the wavelength range of 350-2500 nm with 10 nm spectral resolution. To study the spectral absorption characteristics of the deposits, spectral measurements were carried out at the Department of Earth Sciences, Annamalai University. The samples were powdered and analyzed using the Fourier Transform Infrared (FTIR) spectroscopy method in the CSIL Laboratory, Annamalai University, to understand the spectral absorption characteristics of the iron formations. The samples were further used to study the petrographic characters and geochemical characters of the formations. Microscopic thin-section studies were carried out using a microscope, and major element chemical analyses were carried out by Atomic Absorption Spectroscopy (AAS) analytical techniques at the Department of Earth Sciences, Annamalai University, Chidambaram, Cuddalore District in Tamil Nadu State (Prasanna *et al*., 2009).

RESULTS AND DISCUSSION

Spectral characters of iron and iron-silicate minerals

The quantity of light reflected by a substance is measured by spectral reflectance, represented in photographs by photographic tone or color. It is a result of the materials chemistry and structure being altered by

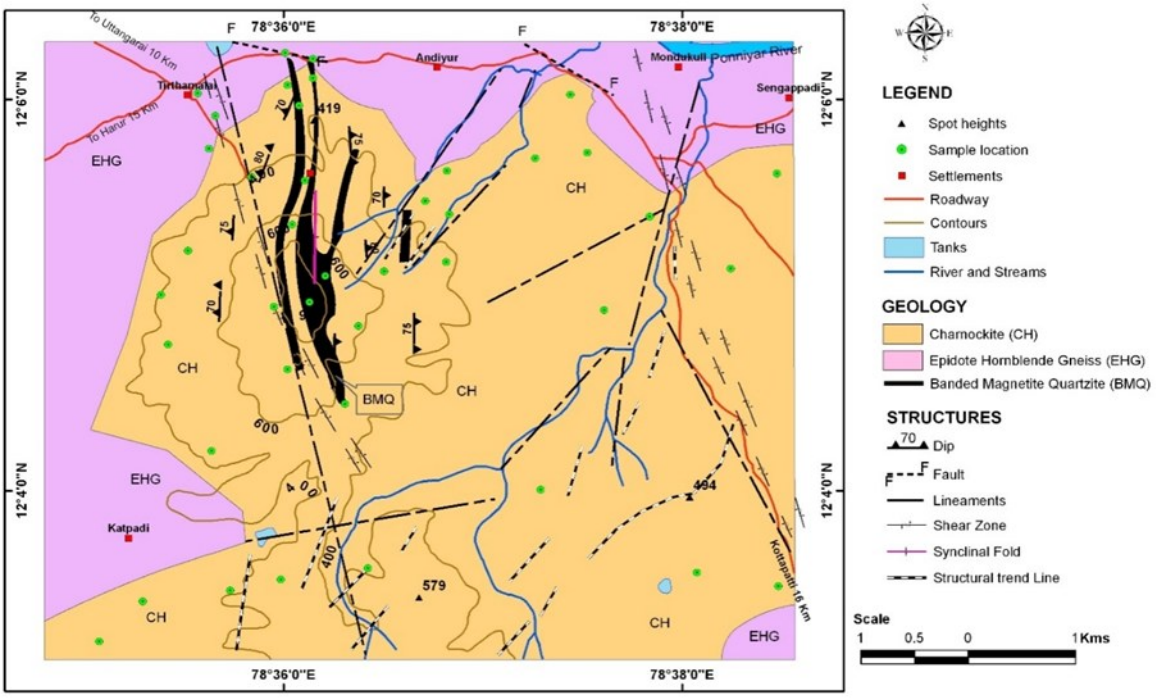

Fig. 1. *Geology map of the study area in Tirthamalai hill showing Charnockite hosts the banded magnetite quartzite in N-S direction in the map.*

physical and environmental causes. Specific minerals absorption properties regulate the spectrum reflectance of rock that results from either electrical or vibrational processes. Charge transfer, when an electron moves from one ion to another ion, and the transition of an electron from one energy level to another inside a metal ion are examples of electronic processes. The mechanisms of vibration involve the banding and stretching of vibrations inside radicals or molecules. Although they are often wider throughout the electronic process, it results in rather crisp absorption characteristics. Opaque minerals such as magnetite and ilmenite have low reflectance spectra due to iron and titanium overlapping element transition and crystal field absorption. Minerals that have low, flat spectral reflectance have been defined as “opaque phases” by Johnson *et al*. (2016). Hematite rich in titanium is predicted as an opaque phase in the near-infrared (IR) wavelength region, as noted by Akinribide *et al*. (2022). Thus, the observation consisted of the role of opaque phases in reducing the intensity of absorption features. On the other hand, rock was poor in hydroxyl-bearing phases. The coarse and fine-grained granites, tonalite, granite, gneiss, and quartzo-feldspathic rocks did not show pronounced absorption in the 2.2 to 2.4 µm wavelength region, even though they are deficient in opaque phases.

Ferrous-iron crystal field absorptions in Fe-bearing aluminosilicates, hornblende and biotite produce broad absorption features centered near 1 µm (Jablonska *et al*., 2021). The recognition of this feature is vital for mapping mafic and ultramafic rocks because it is the only spectral feature common to these major rock types but absent or subdued in felsic and most intermediate rocks (Libeesh *et al*., 2022). The rocks with high content of Fe-bearing aluminosilicates (mafic mylonite, massive amphibolite, each with about 60 vol.% hornblende) had broad, deep absorptions near 1 µm. Felsic rocks, with a low abundance of Fe-bearing aluminosilicates (coarse and fine granite, granite gneiss, quartzo-feldspathic mylonite, and quartz phyllonite, each less than 10 %), lack significant absorptions in the 1µm region. Tonalite had moderate amounts of biotite, and hornblende (10 to 20 vol. % combined for each), showing evidence for weak broad absorption in the 1µm region.

According to Izenberg *et al*. (2014), iron is a metallic element newly formed or worn surface that exhibits substantial absorptions in the visible and near-infrared spectrum. A band of electronic transition is produced by ferrous iron between 1.0 and 1.1 m. Absorption at wavelengths shorter than 0.55 m is caused by charge transfer in the link iron(III) oxide, which is commonly present in weathering products such as iron oxides. This causes the apparent red hue, which is indicative of "iron staining," to appear. Ferric iron exhibits diagnostic spectrum absorptions around the 0.7 and 1.0 m areas, which are crucial in mapping iron ores (Rajendran *et al*., 2007). Ferric minerals most commonly exhibit an absorption band near 0.9 µm due to spin-forbidden transitions in ferric iron (Horgan *et al*., 2014). The most substantial ferrous iron absorption band is usually centered near 1 µm. Ferric iron also causes strong absorptions near 2.4 cm^{-1} (Rajendran and Nasir, 2019). Rajendran and Nasir (2014) used Landsat thematic mapper (TM) images of Oman ophiolite to distinguish rock units. Weathering of elements affecting the spectral response of natural rock surfaces lowered the ferrous iron of absorption at 1.0 m. It is appropriate for use in remote sensing systems because of the occurrence of band variations within weathering elements. Furthermore, the Landsat TM system contained bands on the edge of 0.9-1.1 m ferric and ferrous absorption characteristics that were within the short-wavelength ferric iron cut-off.

Raja *et al*. (2010) generated USGS digital spectral library for the magnetite grains results show typically an opaque spectrally featureless mineral in the visible and near infrared and absorption 0.45 µm and 1.1µm. Fallacaro and Calvin (2003), Kumar *et al*. (2015), and Frei *et al*. (2018) investigated the spectral and chemical properties of banded iron formation in the VNIR, SWIR, and Thermal infrared (TIR) areas. As previously stated, the oxide facies was mostly composed of hematite with little magnetite. The VNIR minima in the thinly banded hematite that occurred in a typical banded iron structure were 0.65 and 0.85 m. The absence of characteristics in the VNIR region might be attributed to a high concentration of magnetite in the sample. In the VNIR/SWIR, the magnetite samples display a typical spectrum. Rajendran *et al*. (2007); Chellamuthu Ranganathan and Siddan (2021); Kanth and Ganaraj (2022) investigated the FTIR spectra of magnetite mineral in magnetite ore powders obtained from the Salem area. They discovered a strong magnetite ore absorption peak at 1085cm^{-1}.Thangavelu *et al*. (2011); Panda *et al*. (2021) observed at Noamundi and Joda Mines, eastern India, that the primary spectral characteristics of iron ores lie in the 850 to 900 nm and 650–750 nm regions.

Hyperspectral signatures of iron ores

The results of the measurement of spectra in the narrower hyperspectral bands over the samples having variations in different grain sizes (fine, less than 0.1 mm; medium, 0.2 to 0.6 mm and coarse, 0.7 to 1.6) are given in Fig. 2. It showed strong absorptions near 500 nm, 900 nm and 2400 nm wavelength regions (Fig. 2 a, b and c). The absorptions were characteristic of the samples' physical, optical and chemical properties,

Table 1. Absorption field of ferrous and ferric iron components

Electronic process	Ferrous (Fe^{2+})	Ferric (Fe^{3+})
Charge transfer		250 nm, 400 nm, 600 nm
Crystal field effects	900-1100 nm, 550 nm 450 nm	750-950 nm, 550-650 nm, 450 nm

mainly the contents of iron formations such as magnetite and silicate minerals and their grain sizes. Such observation of spectral characteristics is comparable to Lake Superior's oxide facies banded iron formation, consisting of hematite with minor magnetite (Fallacaro and Calvin, 2003).

The study showed that the magnetite ore had a strong absorption VNIR/SWIR region of 0.5 µm, 0.9 µm, 1.3 µm and 2.3 µm. The interpretation of absorption characters of the samples of different grain sizes showed significant variations in the absorptions mainly due to its mineral contents viz., i). The fine-grained type, which consisted of magnetite 47 % and quartz 53 %) showed low reflection in the ranges of 0.149 to 0.239 % (Fig. 2a). ii). The medium-grained type has the magnetite 41 % and quartz 59 %, and iii) The coarse-grained type has magnetite 32 % and quartz 68 %) have reflectance percentage ranges of 0.235 % to 0.381 % (Fig. 2b) and 0.221 % to 0.489 % (Fig. 2c) respectively. The low reflection percentage (Fig. 2a) was due to the presence of high magnetite and low quartz minerals in the samples. In comparison, the increase in reflectance (Fig. 2b and 2c) was due to the presence of high quartz and low magnetite in the samples. The high amount of silica concentration determines a higher amount of reflectance and a low amount of absorption in the spectra. The important mineralogical variations can be recognized in the spectra. The spectra of the fresh surfaces of the formations collected from the field were quenched due to abundant magnetite. The quenching effects of the magnetite were reduced by weathering and oxidation to hematite showing characteristic features near 0.9 µm. However, the oxidation of hematite reduced the quenching effects of this mineral and allowed the characteristic absorption features of the primary mineralogy of the rock.

This ferrihydrite spectra displayed a significant water band at 1.44 and 1.93 m, as well as a conspicuous Fe^{3+} band around 0.93 m. There was a shoulder about 0.6 m and a faint wide band near 0.97 m in the maghemite spectra. This sample had some maghemite, as seen by the hematite spectrums band around 0.9 m with a shoulder near 0.6 m. A faint band at 1.1 m and extremely low reflectance were present in the magnetite spectra. The below Table. 1 shows the absorbtions fields of the ferrous and ferric iron component ranges.

The reflectance spectrum of magnetite in the Fig. 2 shows that most of the features are anticipated due to the high proportion of ferric and ferrous contents in the magnetite and hematite minerals in the formations. Rajendran and Nasir (2014) studied the natural surfaces of parts of Oman. They stated that the ferrous iron absorption 1.0 µm is reduced as a result of weathering of minerals controlling the spectral response of natural rock surfaces. The absorption features observed in the narrower hyperspectral bands were significant to map magnetite ores and understanding the concentration of magnetite and the quality of deposits. Despite changes in particle size (i.e., in texture and roughness of the surface), the spectral fingerprints of magnetite ores recorded at several sites for varied grain sizes exhibited relatively low reflectance values, according to a com-

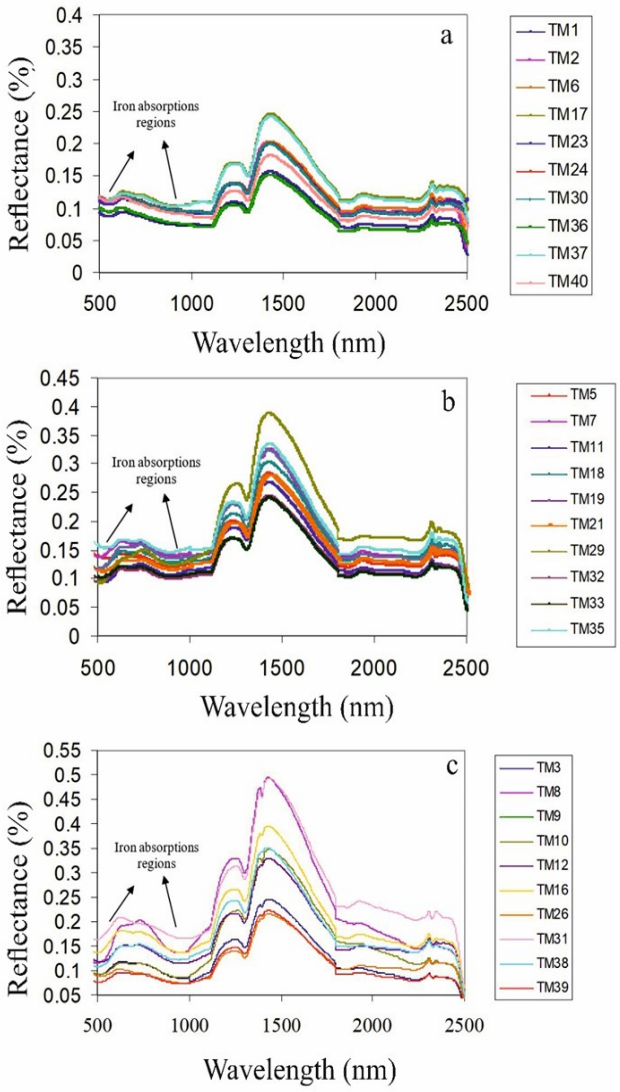

Fig. 2. ***a**) Laboratory spectra of fine-grained **b**) Medium grained and **c**) Coarse-grained type of magnetite quartzite iron ore samples. Black arrow shows the absorption reflectance of iron minerals*

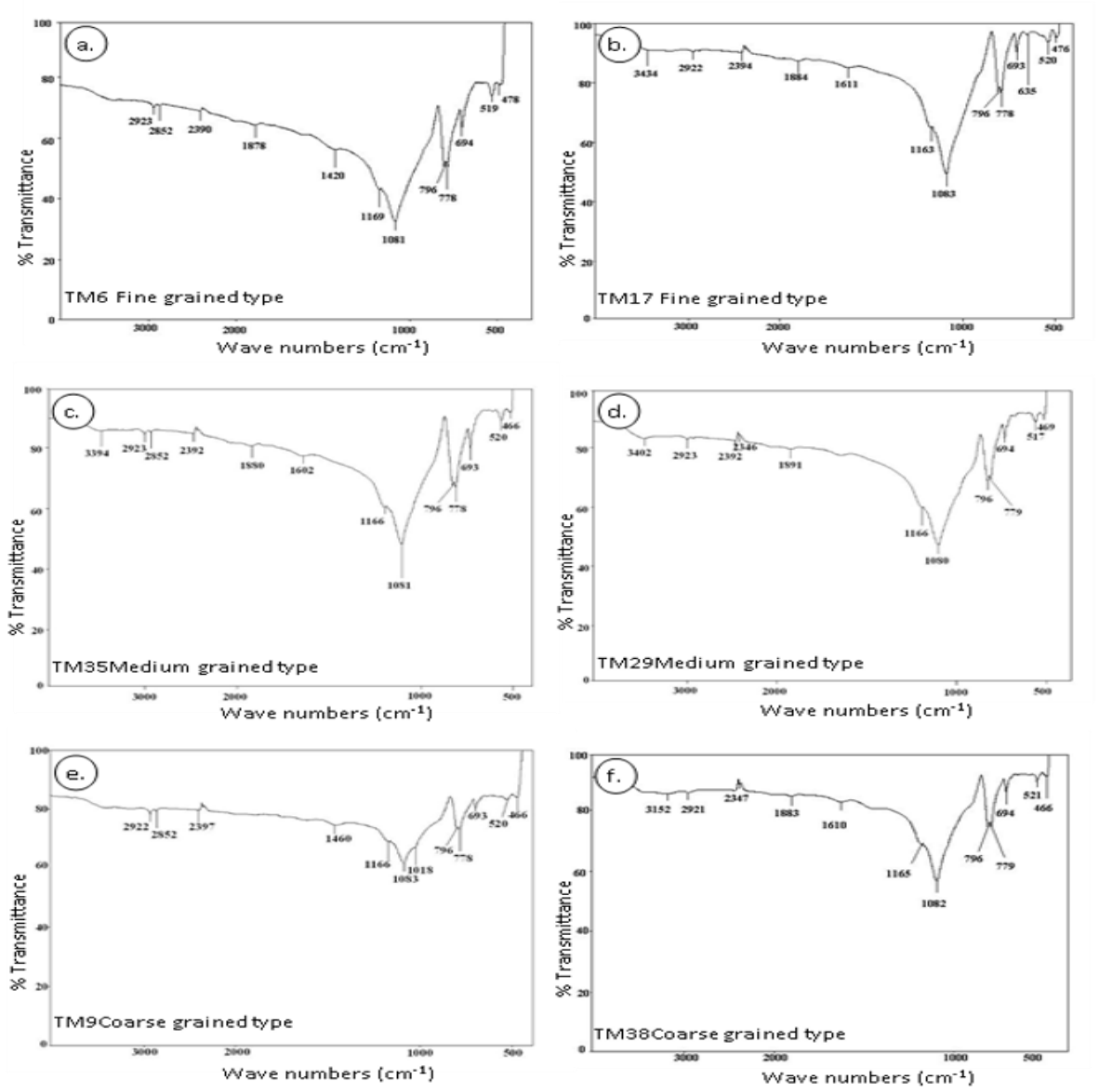

Fig. 3. *FTIR spectra of iron ore samples of Tirthamalai region*

parison between grain size analyses and the obtained spectra.

Fourier Infrared Transform Spectroscopy (FTIR) study

To validate the spectral absorption characteristics of the iron ore formations, the samples were further studied under FTIR spectroscopy. Using the standard analytical procedures, about 20 powdered samples were analyzed by the method, and the results of selected samples are given in (Fig. 3). The spectra of the samples exhibit strong transmittance in the visible and infrared regions between 517 cm^{-1}–521 cm^{-1}, and 1080 cm-1–1083 cm^{-1}, respectively. Gholizadeh *et al.* (2021) and Dibb *et al*. (2022) stated that the transmittance features are comparable to the absorption features studied in the spectra collected in the laboratory sample using a portable Spectroradiometer, which showed the absorptions in the wavelengths of 500 and 900 nm of visible and near-infrared wavelength region.

The transmittance in the ranges 517 cm^{-1} – 521 cm^{-1} and 778 cm^{-1} - 796 cm^{-1} are due to the crystal field effects of ferric iron in the magnetite minerals. Whereas the transmittance in the ranges of 1080 cm^{-1} – 1083 cm $^{-1}$ is due to the crystal field effects of ferrous iron in the hematite (magnetite oxidized) minerals in the samples (Sahoo and Hota., 2018). The fine-grained type of samples (Fig. 4a and b), which had a high amount of magnetite, showed high absorption in the transmittance, whereas the absorption decreased with the increase of grain size and decrease of magnetite contents.

Geochemical signatures

To confirm the spectral absorption characteristics of the iron formations, the field samples were studied in the laboratory. In hand specimens, the magnetites are ex-

hibited black and magnetic, metallic lustre, compact with high hardness and specific gravity. The samples have been classified based on grain sizes as Fine, Medium, and Coarse-grained types (Fig. 4)

Under the microscope, the minerals that occurred in the samples were quartz, magnetite, hematite, limonite, grunerite and hypersthene. The predominant minerals were quartz, magnetite and hematite. The amount of quartz and magnetite varied between more comprehensive limits. To study the chemical characteristics of the formations, the samples were analysed further for the concentration of major chemical elements.

The results of the analyses are given in Tables 2 (a), (b) and (c). It showed that the distribution of Fe_3O_4 contents ranged from 45.52 to 57.25 % (average of 49.27 %); SiO_2 ranging from 41.44 to 53.82 % (average of 47.12 %); Al_2O_3 contents ranging 0.06 % to 1.08 % (average of 0.19 %); MnO contents ranging from 0.01-0.14 % (average of 0.04); MgO contents ranging from 0.05 to 1.69 %, (average 0.52 %); CaO, Na_2O, and K_2O, ranging from 0.08 to 1.98 ; (average 0.42); 0.02 to 0.22 %; (average 0.07); 0.01 to 0.18 %; (average 0.03); TiO_2 and P_2O_5 (0.05 %); (average 0.02 %); 0.41 %; (average 0.13) respectively. The Fe_3O_4 and SiO_2 contents of the samples were significantly high (40-60 weight %), reflecting the superiority of magnetite and quartz. Among the major oxides, such as CaO, K_2O, MgO, MnO, Na_2O and TiO_2 were less than 0.1 % weight. Above the results showed that the samples had a significant amount of iron and silica (Fig. 5), reflecting

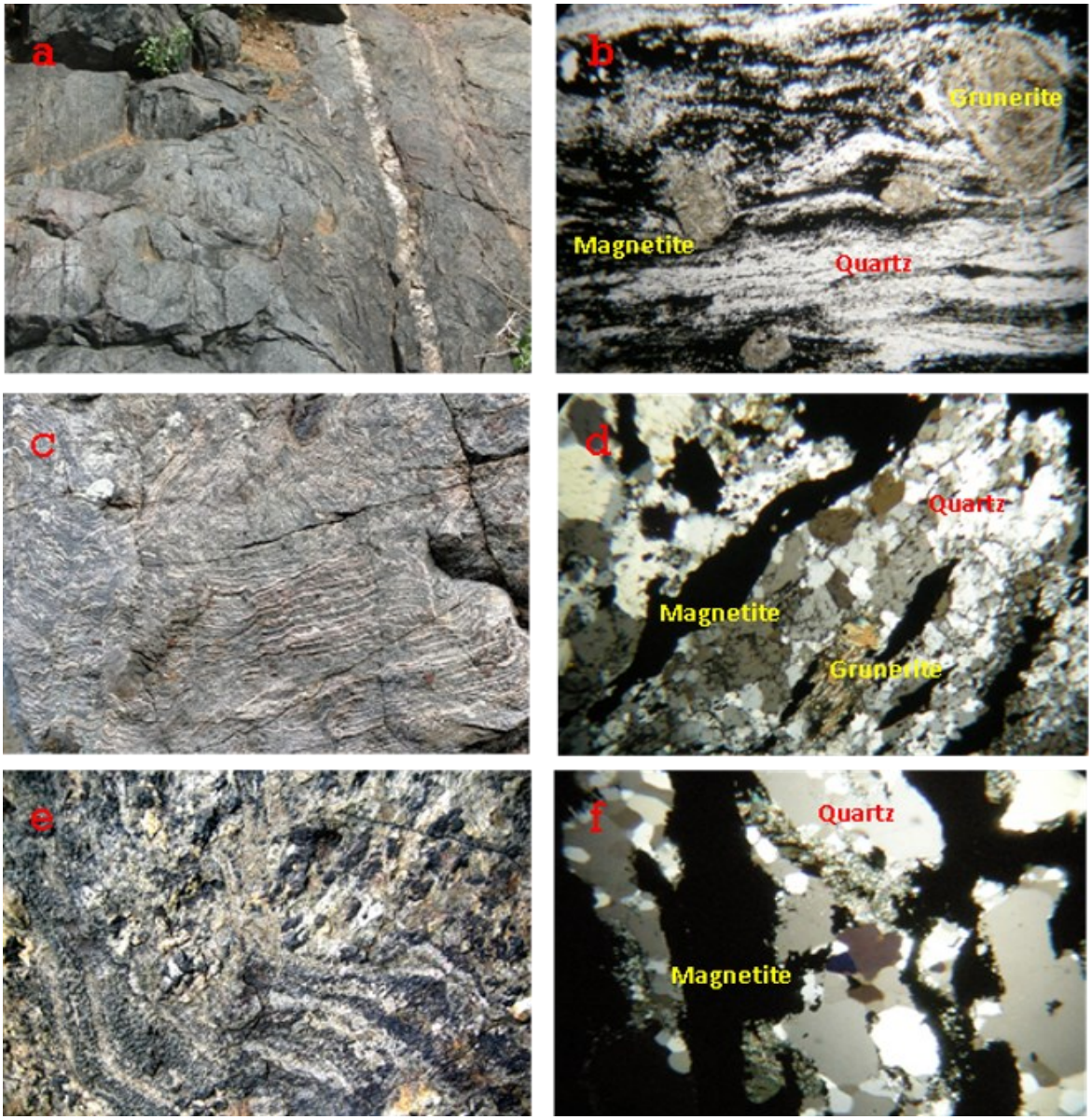

Fig. 4. *Showing the field photographs and microphotographs (Nicol Crossed, 35X). (a) and (b) the fine, (c) and (d) the medium, and (e) and (f) the coarse-grained type samples showing the presence of discontinuous magnetite band, quartz ribbons and grunerite minerals in the iron formations of Tirthamalai region. Photographs a) showing the 10cm width of quartz bands segregated from the fine BMQ*

Table 2. Major elements composition of (a) the fine, (b) the medium and (c) the coarse-grained type samples of the iron ores of Tirthamalai region

A. Fine grained type

Elements	TM1	TM2	TM6	TM17	TM23	TM24	TM30	TM36	TM37	TM40
SiO_2	43.16	44.75	42.96	46.08	43.07	42.63	41.44	43.32	42.53	41.98
Al_2O_3	0.11	0.19	0.26	0.25	0.11	0.22	0.09	0.1	0.08	0.13
Fe_3O_4	55.01	53.34	54.43	52.06	55.05	55.19	57.25	53.06	55.05	55.56
MnO	0.023	0.052	0.14	0.05	0.045	0.051	0.052	0.064	0.075	0.043
MgO	0.66	0.59	0.43	0.56	0.45	0.68	0.05	1.69	1.23	1.16
CaO	0.25	0.28	0.31	0.35	0.52	0.64	0.1	0.39	0.08	0.62
Na_2O	0.06	0.08	0.03	0.08	0.07	0.09	0.05	0.03	0.08	0.05
K_2O	0.02	0.04	0.04	0.03	0.02	0.03	<0.01	0.02	0.05	0.01
TiO_2	0.0355	0.026	0.019	0.05	0.032	0.027	0.028	0.034	0.019	0.016
P_2O_5	0.12	0.15	0.19	0.26	0.13	0.14	0.11	0.17	0.16	0.16
Total	99.44	99.49	98.79	99.77	99.49	99.69	99.17	98.87	99.35	99.72

B. Medium grained type

Elements	TM5	TM7	TM11	TM18	TM19	TM21	TM29	TM32	TM33	TM35
SiO_2	47.18	48.14	49.16	44.28	47.65	49.18	48.88	47.41	45.85	46.99
Al_2O_3	0.05	0.24	0.14	0.12	0.11	0.13	0.14	0.25	0.07	0.16
Fe_3O_4	51.45	49.79	49.04	51.65	49.96	49.15	50.02	51.12	50.34	49.3
MnO	0.039	0.025	0.059	0.03	0.054	0.042	0.029	0.04	0.073	0.046
MgO	0.24	0.54	0.48	0.56	0.78	0.61	0.09	0.24	0.67	1.32
CaO	0.35	0.22	0.7	0.4	0.46	0.35	0.59	0.36	1.98	0.53
Na_2O	0.22	0.04	0.03	0.06	0.05	0.02	0.07	0.06	0.08	0.13
K_2O	0.02	0.02	0.04	0.01	0.02	<0.01	<0.01	0.05	0.02	0.05
TiO_2	0.022	0.032	0.022	0.019	0.012	0.016	0.024	0.031	0.01	0.048
P_2O_5	0.41	0.022	0.001	0.21	0.33	0.16	0.15	0.16	0.24	0.06
Total	99.98	99.06	99.67	97.33	99.42	99.65	99.99	99.72	99.33	98.63

C. Coarse grained type

Elements	TM3	TM8	TM9	TM10	TM12	TM16	TM26	TM31	TM38	TM39
SiO_2	50.96	49.58	49.55	49.32	50.53	49.16	50.66	53.82	51.95	51.51
Al_2O_3	0.21	0.25	0.28	0.18	1.08	0.25	0.18	0.19	0.17	0.15
Fe_3O_4	47.25	47.92	47.83	47.56	47.59	48.73	48.52	45.52	47.3	46.16
MnO	0.069	0.052	0.019	0.03	0.036	0.04	0.028	0.025	0.05	0.034
MgO	0.23	0.25	0.45	0.53	0.42	0.51	0.06	0.059	0.16	0.05
CaO	0.36	0.68	0.46	0.43	0.16	0.45	0.16	0.19	0.09	0.14
Na_2O	0.1	0.08	0.15	0.06	0.08	0.06	0.08	0.05	0.084	0.06
K_2O	<0.01	0.012	0.18	0.019	0.01	0.019	0.02	0.02	0.039	0.039
TiO_2	0.02	0.0019	0.018	0.034	0.018	0.022	0.019	0.019	0.015	0.012
P_2O_5	0.16	0.027	0.035	0.009	0.002	0.027	0.09	0.1	0.07	0.18
Total	99.5	98.87	98.2	99.44	97.92	98.27	99.3	99.53	99.02	99.23

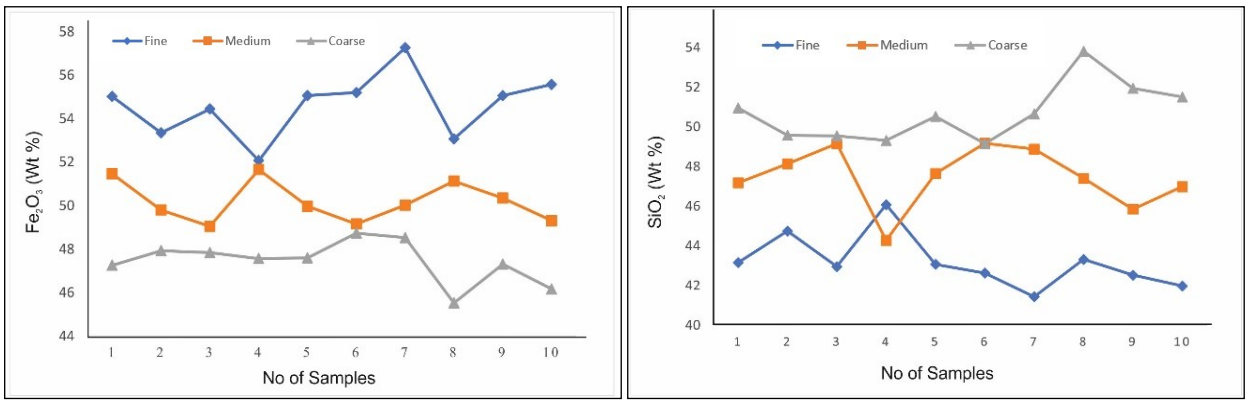

Fig. 5. *Showing the concentration and distribution of (**a**). the Fe_2O_3 (ferric oxide) and (**b**). the SiO_2 in the fine, medium and coarse-grained types of samples of the iron ore deposits of the Tirthamalai region*

the magnetite and quartz minerals that are characterized by the absorptions in the spectra.

Conclusion

The spectral absorption characteristics of the iron ore formations in the Tirthamalai hill in Dharmapurai District, Tamil Nadu carried out through the measurement of laboratory spectral signatures in the wavelength of 350-2500 nm and validated by FTIR analytical study showed that the absorption features around 0.5 µm and 0.9 µm were due to iron contents in the samples. The FTIR spectrum of magnetite samples exhibited strong absorptions in the visible and near-infrared regions showing magnetite in the range of 517 cm^{-1} – 521 cm^{-1} and quartz in the range of 1080 cm^{-1} – 1083 $cm^{-1,}$ respectively. The absorption characteristics of the iron ore samples were confirmed by petrological and geochemical studies, which showed the presence of a high amount of the major iron and silicate minerals such as magnetite, quartz, grunerite and hypersthene. The major elements geochemistry of the samples reflected the high amount of iron and silica in the samples, which caused the spectral absorption in the wavelength. The study showed that the spectral absorption features of the iron formation depend mainly on the banded iron ore formations' physical, optical, and chemical characteristics. The mineralogical identification from hyperspectral images may improve grade control on an iron ore mine face. It will be extremely useful for mining businesses in the near future.

ACKNOWLEDGEMENTS

The author thanks Periyar University, Salem-11, Tamil Nadu, India for providing the University Research Fellowship (URF) during this study.

Conflict of interest

The authors declare that they have no conflict of interest.

REFERENCES

1. Abubakar, A. J. A. Hashim, M. & Pour, A. B. (2019). Identification of hydrothermal alteration minerals associated with geothermal system using ASTER and Hyperion satellite data: a case study from Yankari Park, NE Nigeria. G*eocarto International*, 34(6), 597-625. https://doi.org/10.1080/10106049.2017.1421716
2. Akinribide, O. J. Mekgwe, G. N. Akinwamide, S. O. Gamaoun, F. Abeykoon, C. Johnson, O. T. & Olubambi, P. A. (2022). A review on optical properties and application of transparent ceramics. *Journal of Materials Research and Technology*. 21, 712-738. https://doi.org/10.1016/j.jmrt.2022.09.027
3. Baissa, R. Labbassi, K. Launeau, P. Gaudin, A. & Ouajhain, B. (2011). Using HySpex SWIR-320m hyperspectral data for the identification and mapping of minerals in hand specimens of carbonate rocks from the Ankloute Formation (Agadir Basin, Western Morocco). *Journal of African Earth Sciences*, 61(1), 1-9. https://doi.org/10.1016/j.jafrearsci.2011.04.003
4. Bodsworth, C. (2018). *The extraction and refining of metals*. Routledge. https://doi.org/10.1201/9780203736722
5. Chellamuthu Ranganathan, P. & Siddan, A. (2021). Application of spectral signature to analyze quality of magnesite ore mineral deposits and altered rocks of Salem, India. *Arabian Journal of Geosciences*, *14*(7), 1-20. https://doi.org/10.1007/s12517-021-06963-1
6. Dibb, S. D., Bell III, J. F., & Garvie, L. A. (2022). Spectral reflectance variations of aubrites, metal□rich meteorites, and sulfides: Implications for exploration of (16) Psyche and other “Spectrally featureless” asteroids. *Meteoritics & Planetary Science*, *57*(8), 1570-1588. https://doi.org/10.1111/maps.13891
7. Fallacaro, A. & Calvin, W. (2003, July). Spectral and chemical characteristics of Lake Superior banded iron formation: Analog for Martian hematite outcrops. *In Sixth International Conference on Mars* (p. 3067).
8. Frei, M., Schodlok, M. C., Blumberg, A., & Altermann, W. (2018, December). Hyperspectral Imaging Airborne Campaign (VNIR-SWIR-TIR) in South Africa-Mineral resources applications. In *AGU Fall Meeting Abstracts* (Vol. 2018, pp. GC12A-04).
9. Ganesh, B. P. Aravindan, S. Raja, S. & Thirunavukkarasu, A. (2013). Hyperspectral satellite data (Hyperion) preprocessing – a case study on banded magnetite quartzite in Godumalai Hill, Salem, Tamil Nadu, India. *Arabian Journal of Geosciences*, 6(9), 3249-3256. https://doi.org/10.1007/s12517-012-0584-8
10. Gholizadeh, A., Neumann, C., Chabrillat, S., van Wesemael, B., Castaldi, F., Borůvka, L., ... & Hohmann, C. (2021). Soil organic carbon estimation using VNIR–SWIR spectroscopy: The effect of multiple sensors and scanning conditions. *Soil and Tillage Research*, *211*, 105017. https://doi.org/10.1016/j.still.2021.105017
11. Horgan, B. H. Cloutis, E. A. Mann, P. & Bell III, J. F. (2014). Near-infrared spectra of ferrous mineral mixtures and methods for their identification in planetary surface spectra. *Icarus*, 234, 132-154. https://doi.org/10.1016/j.icarus.2014.02.031
12. Izenberg, N. R. Klima, R. L. Murchie, S. L. Blewett, D. T. Holsclaw, G. M. McClintock, W. E. ... & Dyar, M. D. (2014). The low-iron, reduced surface of Mercury as seen in spectral reflectance by messenger. *Icarus*, 228, 364-374. https://doi.org/10.1016/j.icarus.2013.10.023
13. Jablonska, M. Rachwal, M. Wawer, M. Kadziolka-Gawel, M. Teper, E. Krzykawski, T. & Smolka-Danielowska, D. (2021). Mineralogical and chemical specificity of dusts originating from iron and non-ferrous metallurgy in the light of their magnetic susceptibility. *Minerals*, 11(2), 216. https://doi.org/10.3390/min11020216
14. Jha, E. (2021). Studies on Utilization and Recycling of Steel Plant Fines by Agglomeration (*Doctoral dissertation, Maharaja Sayajirao University of Baroda -India)*.
15. Johnson, J. R. Bell III, J. F. Bender, S. Blaney, D. Cloutis, E. Ehlmann, B. ... & Wiens, R. C. (2016). Constraints on iron sulfate and iron oxide mineralogy from ChemCam

visible/near-infrared reflectance spectroscopy of Mt. Sharp basal units, Gale Crater, Mars. *American Mineralogist*, 101(7), 1501-1514. https://doi.org/10.2138/am-2016-5553

16. Kanth, A. P. & Ganaraj, K. (2022). Spectroscopic and x-ray based microstructural investigation of the early-harappan potsherds and estimation of firing temperature from Kunal Archaeological site, India. *International Journal of Conservation Science*, *13*(1), 131-146.
17. Khan, M. J. Khan, H. S. Yousaf, A. Khurshid, K. & Abbas, A. (2018). Modern trends in hyperspectral image analysis: *A review*. *Ieee Access*, 6, 14118-14129. https://doi.org/10.1109/ACCESS.2018.2812999
18. Kumar, C., Shetty, A., Raval, S., Sharma, R. & Ray, P. C. (2015). Lithological discrimination and mapping using ASTER SWIR Data in the Udaipur area of Rajasthan, India. *Procedia Earth and Planetary Science*, *11*, 180-188. https://doi.org/10.1016/j.proeps.2015.06.022
19. Libeesh, N. K. Naseer, K. A. Arivazhagan, S. Mahmoud, K. A. Sayyed, M. I. & Alqahtani, M. S. (2022). Multispectral remote sensing for determination the Ultra-mafic complexes distribution and their applications in reducing the equivalent dose from the radioactive wastes. *The European Physical Journal Plus*, 137(2), 267. https://doi.org/10.1140/epjp/s13360-022-02473-5
20. Ortenberg, F. (2018). Hyperspectral sensor characteristics: Airborne, spaceborne, hand-held, and truck-mounted; integration of hyperspectral data with Lidar. In Fundamentals, Sensor Systems, *Spectral Libraries, and Data Mining for Vegetation* (pp. 41-69). CRC Press.
21. Panda, S., Jain, M. K., Jeyaseelan, A. T. & Banerjee, K. (2021). Satellite image derived spectral modeling to assess the grades of hematite deposits: a study on Noamundi area in West Singhbhum district, Jharkhand. *Geocarto International*, *36*(3), 299-319. https://doi.org/10.1080/10106049.2019.1594395
22. Prasanna, M. V., Chidambaram, S., Nagarajan, R., Elayaraja, A., & Rajalingam, S. (2009). A Study on Trace Metal Pollution in the Gadilam River Basin, Tamil Nadu, India. *Recent Trends In Water Research-Hydrogeochemical And Hydrological Perspective*, 67-73.
23. Raja, S. Rajendran, S. Ganesh, P. B. & Thirunavukkarasu, A. (2010). Study on hyperspectral signatures for magnetite iron ore in Thattayengerpet region of Trichirappalli district in Tamil Nadu State, India. *International Journal of Geomatics and Geosciences*, 1(2), 188.
24. Rajendran, S. & Nasir, S. (2014). Hydrothermal altered serpentinized zone and a study of Ni-magnesioferrite–magnetite–awaruite occurrences in Wadi Hibi, Northern Oman Mountain: Discrimination through ASTER mapping. *Ore Geology Reviews*, 62, 211-226. https://doi.org/10.1016/j.oregeorev.2014.03.016
25. Rajendran, S. & Nasir, S. (2019). ASTER capability in mapping of mineral resources of arid region: A review on mapping of mineral resources of the Sultanate of Oman. *Ore Geology Reviews*, 108, 33-53. https://doi.org/10.1016/j.oregeorev.2018.04.014
26. Rajendran, S. Thirunavukkaraasu, A. Poovalingaganesh, B. Kumar, K. V. & Bhaskaran, G. (2007). Discrimination of low-grade magnetite ores using remote sensing techniques. *Journal of the Indian Society of Remote Sensing*, 35(2), 153-162.
27. Rajendran, S. Thirunavukkarasu, A. Balamurugan, G. & Shankar, K. (2011). Discrimination of iron ore deposits of granulite terrain of Southern Peninsular India using ASTER data. *Journal of Asian Earth Sciences*, 41(1), 99-106. https://doi.org/10.1016/j.jseaes.2011.01.004
28. Roonwal, G. S. (2018). *Mineral exploration:Practical application*. Springer Singapore.
29. Sahoo, S. K. & Hota, G. (2018). Surface functionalization of GO with MgO/MgFe2O4 binary oxides: a novel magnetic nanoadsorbent for removal of fluoride ions. *Journal of Environmental Chemical Engineering*, 6(2), 2918-2931. https://doi.org/10.1016/j.jece.2018.04.054
30. Santosh, M. Maruyama, S. & Sato, K. (2009). Anatomy of a Cambrian suture in Gondwana: Pacific-type orogeny in southern India?: *Gondwana Research*, v. 16, p. 321-341. https://doi.org/10.1016/j.gr.2008.12.012
31. Santosh, M. Yang, Q.Y. Shaji, E. Tsunogae, T. Mohan, M.R. & Satyanarayanan, M. (2015). An exotic Mesoarchean 739 microcontinent: the Coorg Block, southern India. *Gondwana Research*, 27(1): 165–195. https://doi.org/10.1016/j.gr.2013.10.005
32. Sylvestre, G. Laure, N. T. E. Djibril, K. N. G. Arlette, D. S. Cyriel, M. Timoleon, N. & Paul, N. J. (2017). A mixed seawater and hydrothermal origin of superior-type banded iron formation (BIF)-hosted Kouambo iron deposit, Palaeoproterozoic Nyong series, Southwestern Cameroon: constraints from petrography and geochemistry. *Ore Geology Reviews*, 80, 860-875. https://doi.org/10.1016/j.oregeorev.2016.08.021
33. Thangavelu, M. Shanmugam, S. & Bhattacharya, A. K. (2011). Hyperspectral radiometry to quantify the grades of iron ores of Noamundi and Joda mines, Eastern India. *Journal of the Indian Society of Remote Sensing*, 39 (4), 473-483. https://doi.org/10.1007/s12524-011-0109-z
34. Thirunavukkarasu, A. Rajendran, S. Suresh, R. Sakthivel, C. Kasilingam, C. & Sankar, M. (2015). Geochemistry Of Iron Ore Deposits of Tirthamalai Area, Dharmapuri District, Tamilnadu, India-Implication on the Genesis. *Journal of Applied Geochemistry*, 17(4), 462-470.
35. Tsunogae, T. & Santosh, M. (2010). Sapphirine + quartz assemblage from the Southern Granulite Terrane, India: diagnostic evidence for ultrahigh-temperature metamorphism within the Gondwana collisional orogen. *Geological Journal,* https://doi.org/10.1002/gj.1244doi: 10.1002/gj.1244.